© 2017. Published by The Company of Biologists Ltd | Journal of Cell Science (2017) 130, 3507-3516 doi:10.1242/jcs.201657

RESEARCH ARTICLE

Drosophila Atlastin in motor neurons is required for locomotion and presynaptic function

Cristian De Gregorio[1,2], Ricardo Delgado[3], Andrés Ibacache[1,2], Jimena Sierralta[1,2] and Andrés Couve[1,2,*]

ABSTRACT

Hereditary spastic paraplegias (HSPs) are characterized by spasticity and weakness of the lower limbs, resulting from length-dependent axonopathy of the corticospinal tracts. In humans, the HSP-related atlastin genes *ATL1–ATL3* catalyze homotypic membrane fusion of endoplasmic reticulum (ER) tubules. How defects in neuronal Atlastin contribute to axonal degeneration has not been explained satisfactorily. Using *Drosophila*, we demonstrate that downregulation or overexpression of Atlastin in motor neurons results in decreased crawling speed and contraction frequency in larvae, while adult flies show progressive decline in climbing ability. Broad expression in the nervous system is required to rescue the *atlastin*-null *Drosophila* mutant (*atl*^{2}) phenotype. Importantly, both spontaneous release and the reserve pool of synaptic vesicles are affected. Additionally, axonal secretory organelles are abnormally distributed, whereas presynaptic proteins diminish at terminals and accumulate in distal axons, possibly in lysosomes. Our findings suggest that trafficking defects produced by Atlastin dysfunction in motor neurons result in redistribution of presynaptic components and aberrant mobilization of synaptic vesicles, stressing the importance of ER-shaping proteins and the susceptibility of motor neurons to their mutations or depletion.

KEY WORDS: Atlastin, Human spastic paraplegias, Endoplasmic reticulum, Axon, Trafficking, Vesicle, Presynaptic terminal

INTRODUCTION

Hereditary spastic paraplegias (HSPs) constitute a group of genetically diverse disorders with a prevalence of three to 10 per 100,000 individuals, characterized by spasticity and weakness of the lower limbs, resulting from length-dependent axonopathy of the corticospinal tracts. To date, 59 genes (76 loci) have been associated with autosomal dominant, autosomal recessive and X-linked modes of inheritance (Novarino et al., 2014; Klebe et al., 2015). No available treatment exists to cure, prevent or slow the progression of the disease. Gene clusters associated with the disease define protein transport as a convergent and relevant biological process in HSPs. Indeed, mutations in a small number of genes encoding membrane-shaping proteins of the endoplasmic reticulum (ER) cause nearly 65% of autosomal dominant HSP cases. These include spastin, *REEP1*, *TFG*, and the atlastin (*ATL1–ATL3*) and reticulon genes (Blackstone, 2012; Montenegro et al., 2012; Beetz et al., 2013). However, it remains unclear how mutations in these genes affect ER functionality and how they target axonal degeneration.

The ER is a highly conserved and continuous organelle present in all eukaryote cells. It is responsible for the synthesis and modification of the majority of membrane and secreted proteins, lipid synthesis, Ca^{+2} signaling and glucose homeostasis. Structurally, it includes the nuclear membrane, the ribosome-rich rough ER (RER), and the smooth ER (SER) that forms a tubular network containing sparse polyribosomes. The neuronal RER is abundant in the soma and the surrounding somatodendritic volume (González and Couve, 2014), whereas the tubular network of the SER invades distal dendrites and the axon. The structure of the tubular ER is highly dynamic (Vedrenne and Hauri, 2006; Borgese et al., 2006; Shibata et al., 2006). Generation and maintenance of tubules are controlled by their association to the cytoskeleton (Waterman-Storer and Salmon, 1998), and by integral membrane proteins – at least two members of the receptor expression-enhancing proteins (REEPs), i.e. REEP1 and REEP5 in mammals (Yop1 in yeast), and the reticulon proteins (comprising RTN1-4) (Voeltz et al., 2006; Hu et al., 2008; Park et al., 2010). These proteins share two characteristic transmembrane hairpins that are sufficient for the formation of ER tubules *in vitro*. Additionally, Atlastin, a highly conserved dynamin-related GTPase, controls the dynamic structure of the ER network by mediating homotypic fusion of ER tubules (Hu et al., 2009; Orso et al., 2009). Multiple missense mutations in the conserved GTPase domain, transmembrane and other domains of the human atlastin proteins (e.g. ATL1) have been identified in HSP patients (McCorquodale et al., 2011; Guelly et al., 2011), suggesting that ER morphology is a key pathological determinant. However, how the altered ER structure predisposes to HSP and whether defects in neuronal atlastin proteins are necessary and sufficient to produce the disease have not been explained satisfactorily.

A single orthologous *atlastin* gene exists in *Drosophila*. *Drosophila atlastin* (*atl*) is substantially conserved and has the same structural domains as its mammalian isoforms (Orso et al., 2009). Downregulation of Atlastin in larval muscle results in ER fragmentation, while overexpression of Atlastin *in vivo* produces expanded ER structures in motor neurons, possibly due to a GTPase-dependent increase in membrane fusion (Orso et al., 2009). The absence of *atl* results in age-dependent degeneration of dopaminergic neurons in adult flies and abnormal neuromuscular junctions in larvae (Lee et al., 2008, 2009). Both cell autonomous and nonautonomous defects have been associated with muscle degeneration (Xu et al., 2016), but how neuronal Atlastin contributes to the pathogenesis of HSP is less clear. Importantly, owing to its conserved functions, the study of neuronal Atlastin in *Drosophila* could contribute to the understanding of how ER defects produce increased sensitivity to degeneration in lengthy mammalian axons.

Here, we combine *in vivo* modification of Atlastin expression in motor neurons with analysis of locomotor behavior, synaptic function, ultrastructure of synaptic boutons, and distribution of

[1]Department of Neuroscience, Universidad de Chile, Santiago CP8380453, Chile. [2]Biomedical Neuroscience Institute, Faculty of Medicine, Universidad de Chile, Santiago CP8380453, Chile. [3]Department of Biology, Faculty of Sciences, Universidad de Chile, Santiago CP7800003, Chile.

*Author for correspondence (andres@neuro.med.uchile.cl)

A.C., 0000-0003-4216-8672

Received 16 January 2017; Accepted 29 August 2017

Journal of Cell Science (2017) 130, 3507-3516 doi:10.1242/jcs.201657

axonal organelles and presynaptic proteins by confocal microscopy. We demonstrate that disruption of motor neuron Atlastin is sufficient to produce locomotor defects and synaptic dysfunction. Interestingly, these behavioral phenotypes correlate with abnormalities in the supply of presynaptic components and the integrity of spontaneous release and the reserve pool of synaptic vesicles. Our results contribute to the understanding of the neuronal mechanisms of *atl* pathogenesis, and establish a role of neuronal Atlastin in the overall organization of the presynaptic terminal.

RESULTS

Altered levels of Atlastin in motor neurons produce severe locomotion defects in larvae and adults

Mutations in atlastin genes produce severe motor disorders in humans, and alterations of the *Drosophila* orthologue recapitulate many behavioral abnormalities (Zhao et al., 2001; Lee et al., 2008; Summerville et al., 2016; Xu et al., 2016). To address the specific role of neuronal Atlastin in locomotion, we generated flies with downregulated or upregulated Atlastin in motor neurons by expressing UAS-dsRNA-Atlastin and UAS-Atlastin (UAS-Atl) under the control of the specific motor neuron promoters *C380-Gal4* and *OK6-GAL4* (Sanyal, 2009). Two knockdown lines were established: one expressing a long-hairpin dsRNA from Vienna Drosophila Resource Center (VDRC) (dsRNA *atl* 1), and one expressing a short-interfering RNA for *atl* from Bloomington Drosophila Stock Center (BDSC) (dsRNA *atl* 2). We also used two different lines to overexpress *Drosophila* Atlastin (OE95/UAS-Atl1 and OE64/UAS-Atl2; Orso et al., 2009). Efficiency of downregulation was evaluated by real-time quantitative PCR (qPCR) from third instar larvae brain tissue after expressing the dsRNAs under the control of the Elav promoter (*Elav-Gal4*) at 29°C (Fig. S1A). Overexpression levels under the control of the Elav promoter (*Elav-Gal4*) were also determined by qPCR from third instar larvae brains, and by immunofluorescence of Atlastin-myc in motoneurons and segmental nerves under the control of the OK6 promoter (*OK6-Gal4*) (Fig. S1A,C). Additionally, we analyzed the subcellular localization of this fusion protein by co-expressing the ER marker GFP-KDEL in muscle cells (Fig. S1B). We then examined the locomotor behavior in third instar larvae, and in young and aged adults. Both the speed and contraction frequency were significantly reduced in Atlastin-downregulated larvae (Fig. 1A,B). Additionally, a tail-flip phenotype was observed in ∼60% of dsRNA *atl* larvae. Tail-flipping is a feature of axonal transport defects and reminiscent of the loss of function of the motor protein kinesin (Gindhart et al., 1998). Overexpression of Atlastin in larvae grown at 29°C produced even more severe motor deficits (Fig. 1A,B).

atl^2 mutant larvae, as well as the trans-heterozygote larvae with a deficiency covering the *atl* gene (atl^2/DF), also displayed a significant reduction in speed and contraction frequency (Fig. 1C,D). More importantly, pan-neural expression of Atlastin using the Elav promoter significantly improved crawling speed and contraction frequency in atl^2/DF larvae (Fig. 1C,D). For the Atlastin rescue experiments, mutant larvae were grown at 21°C to minimize the locomotor defects caused by Atlastin overexpression. Restoration of locomotor behavior by expression of Atlastin in muscle cells produced similar recovery levels in speed as in neurons, but less recovery in contraction (Fig. 1C,D). Expression of Atlastin exclusively in motor neurons using the specific driver OK6 produced no significant improvements (Fig. 1C,D). By contrast, broader expression of Atl in all glutamatergic or cholinergic neurons produced strong recoveries (Fig. 1C,D). Taken together, these results demonstrate that loss of Atlastin in motor neurons is sufficient to cause locomotor abnormalities in larvae. However, expression of Atl in broader neuronal circuits is required to restore motor capabilities in a mutant background.

In adults, climbing speed was severely reduced in 35-day-old, but not in 5-day-old, flies expressing dsRNA atl in motor neurons, revealing age-dependent locomotor deficits (Fig. 1E). These observations indicate that neuronal Atlastin is necessary for adequate motor behavior in aged flies.

Loss of function of Atlastin in motor neurons impairs synaptic function and reduces vesicle density

Mutations in HSP genes or changes in the abundance of their proteins modify synaptic transmission in *Drosophila* (Sherwood et al., 2004; Trotta et al., 2004; Nahm et al., 2013). We thus evaluated the role of Atlastin in the structure and function of the neuromuscular junction (NMJ) synapse. Because reduction in expression and behavioral responses were equivalent for dsRNA *atl* 1 and 2, we used dsRNA *atl* 1 for the remainder of the study. First we measured bouton number in muscle 6/7 of A2 and A6 larval segments by anti-HRP and anti-Dlg staining and confocal microscopy, as described previously (Miller et al., 2012). Bouton number relative to muscle area increased in Atlastin-downregulated larvae, while overexpression produced a significant decrease (Fig. S2B). Interestingly, satellite bouton number increased in both Atlastin loss- and gain-of-function larvae (Fig. S2C). We did not observe differences in active zone number or density when we measured Bruchpilot distribution and intensity (not shown).

We then examined the ultrastructure of synaptic boutons in larvae by transmission electron microscopy (EM). No gross abnormalities were observed in dsRNA *atl* terminals, which contained abundant synaptic vesicles, mitochondria and active zones (AZs) (Fig. 2A,E). Despite this apparent morphological conservation, quantification of the images revealed a significant reduction in bouton area (Fig. 2F). To begin addressing possible synaptic transmission defects, we quantified the number of synaptic vesicles adjacent (200 nm) or nonadjacent (200–400 nm) to the AZ, as described by Long et al. (2010) (Fig. 2B). The number of vesicles adjacent to the AZ was not different in wild-type and dsRNA *atl*-expressing larvae (Fig. 2C). By contrast, vesicles located further from the AZ were substantially diminished in knockdown larvae compared to wild-type larvae (Fig. 2D). Larger membranous organelles containing smaller vesicle-like structures reminiscent of multivesicular bodies (MVBs) also accumulated in dsRNA *atl*-expressing larvae (Fig. 2G,H). These observations suggest that Atlastin might be involved in the biogenesis, mobilization or accumulation of a pool of synaptic vesicles that is not adjacent to the AZ.

Given the behavioral and ultrastructural consequences of downregulating Atlastin in motor neurons, we next examined whether synaptic function was altered at the NMJ. Frequencies of spontaneous excitatory postsynaptic currents (sEPSCs), but not their amplitudes, were significantly reduced in atl^2, Atlastin deficiency or dsRNA *atl* larvae (Fig. 3A–C). As AZs were not affected, these results suggest a lower availability of the readily releasable pool of synaptic vesicles at low calcium concentration. We next examined the behavior of different vesicular populations at physiological Ca^{2+} concentration using an evoked paradigm. Upon stimulating the nerve with a short tetanus (50 s, 20 Hz), the amplitude of evoked excitatory junctional potential (eEJP) in wild-type larvae was rapidly facilitated, and subsequently depressed until the end of the stimulus when this effect was completely reversed (Fig. 3D, upper trace, and Fig. 3E, recovery, 0.98±0.03 of the initial

Journal of Cell Science (2017) 130, 3507-3516 doi:10.1242/jcs.201657

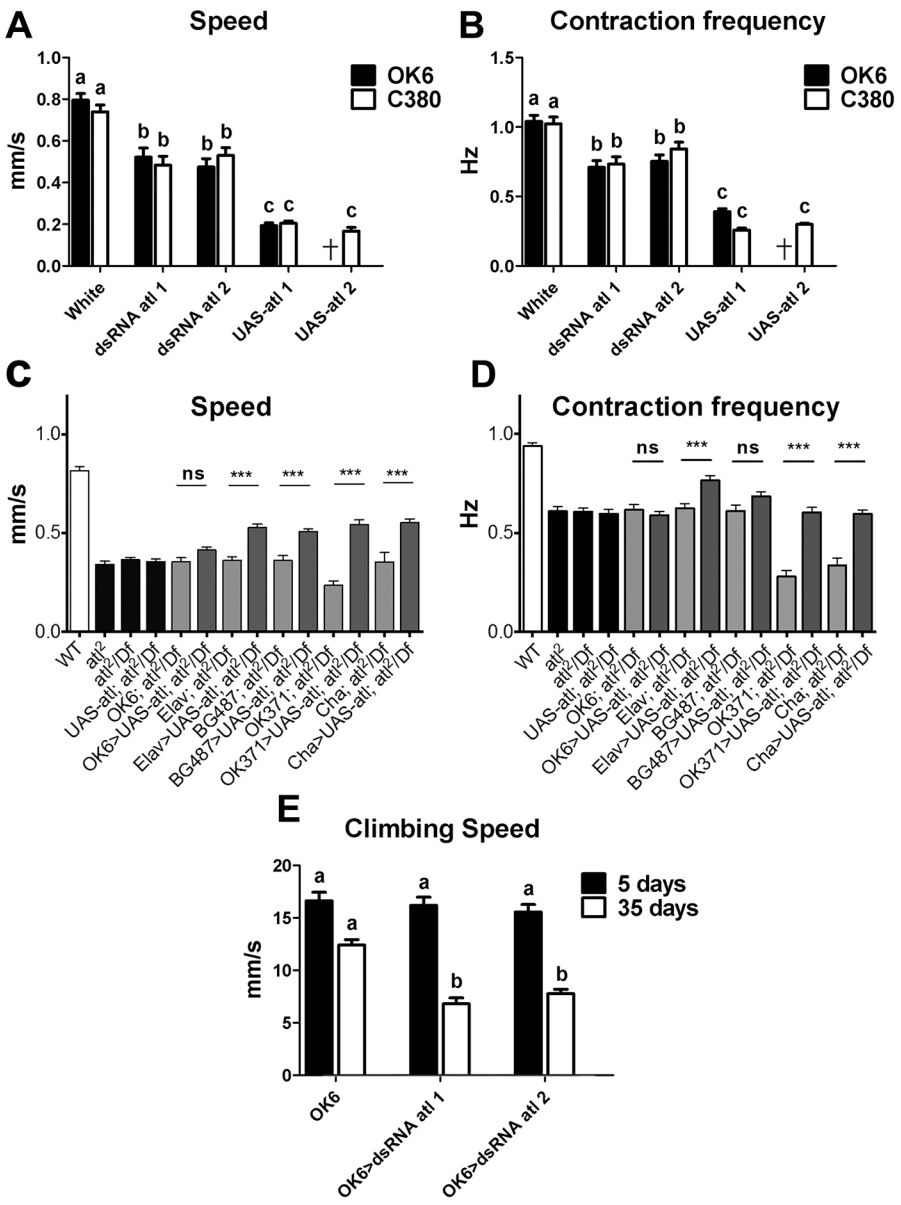

Fig. 1. Changes in Atlastin levels in motor neurons produce severe motor deficits. (A,B) Quantification of the speed (A) and contraction frequency (B) of third instar larvae expressing dsRNA *atl* 1 or 2, or overexpressing Atlastin full-length protein (UAS-Atl 1 or 2), using OK6 (black bars) or C380 (white bars) motor neuron Gal4-drivers (n=21, one-way ANOVA, lower case letters indicate statistical significance of differences between categories). (C,D) Quantification of the speed (C) and contraction frequency (D) in locomotion assays of atl^2, trans-heterozygote deficiency (atl^2/DF) third instar larvae, with motor neuron (OK6), pan-neuronal (Elav), glutamatergic (OK371), cholinergic (Cha) or muscle (BG487) Atlastin rescue (n=18, Student's t-test versus genetic background control). (E) Climbing speed in age-synchronized flies at 5 days (black bars) or 35 days (white bars) after hatching, expressing two different Atlastin dsRNAs (n=36, one-way ANOVA). Data are mean±s.e.m. ***P<0.001; ns, nonsignificant.

amplitude, n=6). Pretetanus eEJP amplitudes (low-frequency stimulation, 1 Hz) in Atlastin-downregulated larvae were similar to controls under these conditions (Fig. S3), and synaptic currents during the tetanus were correspondingly facilitated and depressed. However, eEJPs in dsRNA atl larvae failed to recover completely after the short tetanus (Fig. 3D, lower trace and Fig. 3E, recovery, 0.59±0.12 of the initial amplitude, n=8; P<0.05), suggesting that the reserve pool of synaptic vesicles was not properly mobilized.

We used long tetanic nerve stimulation to reveal the contribution of different vesicular pools through depression decay components (Delgado et al., 2000). Depression of eEJPs in response to high-frequency stimulation in controls occurred through three components: a fast, exponential decay process attributed to the depletion of the docked vesicle pool (τ1: 1.6 s±0.9 s), an intermediate exponential component attributed to the depletion of the readily releasable pool of vesicles (τ2: 13.0±1.8 s), and a slower component attributed to the depletion of the reserve pool (τ 3: 95±50 s; n=5) (Fig. 3F,G, upper trace, and Fig. 3H). The slowest component of eEJP amplitude depression was missing in dsRNA *atl* larvae (Fig. 3F,G, lower trace, and Fig. 3H). Indeed, the eEJP amplitude depression of these synapses occurred through only two exponential decay components (τ1: 0.7±0.1 s; τ2: 21.0±2.5 s; n=5). Recovery after long stimulation was also compromised, as described for the short tetanus paradigm.

Although functional and morphological criteria do not necessarily refer to identical synaptic vesicle pools, combined, these observations are consistent with selective defects in the mobilization of the readily releasable pool and/or the reserve pool in dsRNA *atl* larvae. However, we cannot rule out other mechanisms that could affect synaptic depression, such as differential effects between type1b and type1s boutons, action potential failures or calcium mobilization.

Atlastin is required for proper anterograde secretory trafficking in motor neurons

We next examined the organization of secretory organelles in anterior (shorter axons, A2 level) and posterior (longer axons, A6 level) axons of third instar larvae by confocal microscopy. Because OE95/UAS-Atl1 showed more moderate behavioral effects than OE64/UAS-Atl2, and also produced milder overexpression

Journal of Cell Science (2017) 130, 3507-3516 doi:10.1242/jcs.201657

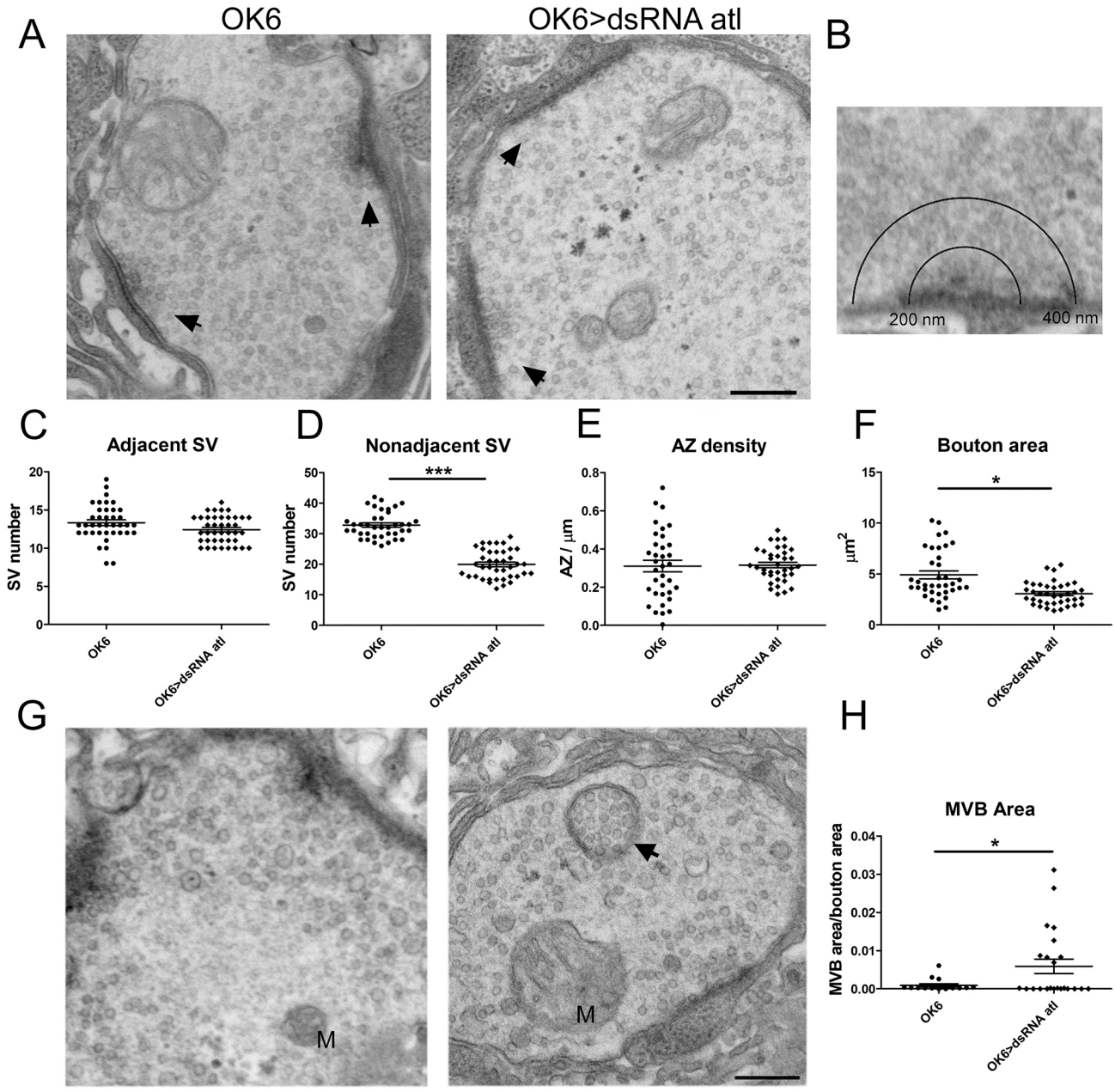

Fig. 2. Atlastin is necessary for synaptic vesicle organization at the NMJ terminal. (A) Representative EM images of synaptic boutons in muscles 6/7 in third instar control or dsRNA *atl* larvae. Arrows indicate the positions of AZs. (B) Adjacent and nonadjacent synaptic vesicle quantification procedure diagram. (C,D) Quantification of adjacent (C) and nonadjacent (D) synaptic vesicles in boutons from control (black circles) or dsRNA *atl* larvae (black diamonds) (*n*=8 larvae, Student's *t*-test for two independent samples). (E,F) Quantification of synaptic bouton area (E) and AZ density (F) from control (black circles) or dsRNA atl larvae (black diamonds) (*n*=8 larvae, Student's *t*-test for two independent samples). (G) Representative EM images of boutons from control and dsRNA *atl* larvae that illustrate the abundance of MVB-like structures in dsRNA atl boutons. M, mitochondria. (H) Quantification of MVB-like structures in control (black circles) or dsRNA *atl* larvae (black diamonds) (*n*=8, Student's *t*-test for two independent samples). Data are mean±s.e.m. **P*<0.05, ****P*<0.001. Scale bars: 200 nm.

(Fig. S1A), this strain was used for the remainder of the study. The ER, revealed by the expression of RFP-KDEL, was prominent in motor neuron somas and appeared as a moderately dense array of puncta along anterior and posterior nerves. The density, but not the size, of puncta was significantly affected in axons of Atlastin-downregulated or -upregulated larvae (Fig. 4A–C). ER exit sites visualized by the expression of Sten-GFP were also distributed as puncta in nerves. Puncta density, but not size, was increased after Atlastin downregulation, whereas size, but not density, was increased upon upregulation (Fig. 4D–F). Larger clusters were observed in neuronal somas for the Golgi complex identified by ManII-GFP, and puncta density and size were increased in axons of both Atlastin-modified animals (Fig. 4G–I). We are aware of the fragmentation of the ER and the possible aggregation of other organelle markers after fixation or overexpression. However, while we cannot state that the punctate distribution of axonal organelles reflects their true appearance *in vivo*, we can conclude that they are modified, directly or indirectly, by Atl expression. Indeed, axonal mitochondria (mito::gfp) and endosome (Rab5-GFP) size and density were unaffected in both genotypes (data not shown).

To determine whether organelle disorganization influenced protein localization, we evaluated the distribution of synaptic

Journal of Cell Science (2017) 130, 3507-3516 doi:10.1242/jcs.201657

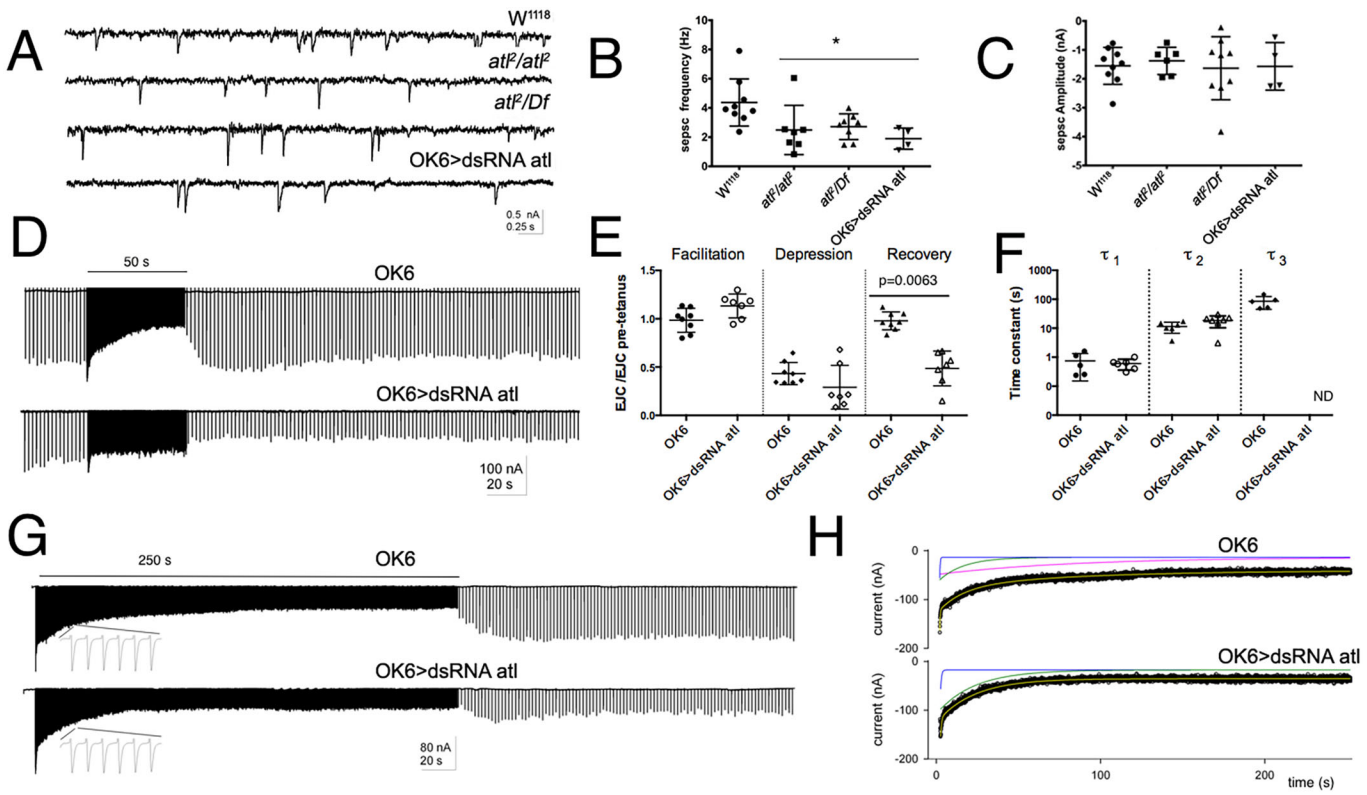

Fig. 3. Atlastin loss of function disrupts synaptic vesicle pools. (A) Representative traces of voltage-clamp recordings of spontaneous excitatory postsynaptic currents (sepsc) in control (wild-type) and loss-of-function Atlastin (*atl*^{2}, deficiency or OK6>dsRNA *atl*). (B,C) Frequency and amplitude of sEPSCs (sepsc) under the conditions shown in A (one-way ANOVA). (D) Representative traces of voltage-clamp recordings of control (OK6) and loss-of-function Atlastin (OK6>dsRNA *atl*) in motoneurons. Recordings show eEJCs elicited in the muscle in response to nerve stimulation, first at 1 Hz, then at 20 Hz/50 s and again at 1 Hz. (E) Quantification of the eEJP (EJC) amplitudes in A, normalized to the amplitude before the tetanus. (F) Decay time constants determined for control and loss-of-function muscles during the stimulus of the nerve at 20 Hz/250 s. ND, not detectable. (G) Representative traces of voltage-clamp recordings of control (OK6) and loss-of-function Atlastin (OK6>dsRNA *atl*) in motoneurons in response to 20 Hz/250 s stimulation. (H) Fitting of a representative recording for control and dsRNA *atl*. Each time constant fit is shown in a different color: τ1, blue; τ2, green; τ3, pink. Fitting using three (top) or two (bottom) constants is shown in yellow. Data are mean±s.e.m. **P*<0.05.

components in all conditions. Endogenous cysteine string protein (CSP), a member of the DnaJ/Hsp40 family of co-chaperones present in synaptic vesicles, accumulated in posterior nerves of Atlastin-downregulated or -upregulated larvae (Fig. 5A,C,D). Importantly, the density of CSP in boutons was significantly decreased in modified animals (Fig. 5B,E). Similar results were obtained with synaptobrevin, a member of the SNARE complex (Fig. 5F–J, Syb-GFP).

Finally, we noticed that Lamp (also known as Lamp1)-GFP, a lysosomal marker, also accumulated in posterior axons, where the size of these structured increased significantly (Fig. 6A–C). To determine whether synaptic proteins were targeted to lysosomes as a consequence of trafficking defects, we examined the co-distribution of accumulated CSP and lysosomes. Importantly, axonal CSP aggregates co-distributed with the lysosomal marker Lamp-GFP (Fig. 6D).

Together, these results support that synaptic proteins fail to accumulate in presynaptic terminals of Atlastin-downregulated larvae, possibly as a result of axonal transport defects and related degradation, although the latter awaits functional confirmation.

DISCUSSION

Our results demonstrate that Atlastin in motor neurons is required for normal locomotor behavior and synaptic function in *Drosophila*. Moreover, they uncover the contribution of Atlastin to the organization of axonal organelles and synaptic proteins that may ultimately lead to defects in the availability of vesicles and presynaptic components in axonal boutons. They also provide direct demonstration that morphological, synaptic and behavioral defects related to the pathogenicity of HSPs, including progressive decline in locomotor behavior, are mimicked by neuron-specific downregulation of Atlastin, contributing to the understanding of the subcellular phenomena underlying motor alterations in mammals and humans. Finally, the accumulation of lysosomes and, possibly, of degrading proteins within these structures raises the possibility that clearance systems might be compromised in long axons, revealing a cellular hallmark of neurodegenerative diseases in *Drosophila* HSP models.

Previous reports indicate that expression of Atlastin in muscle partially rescues the morphological defects of the NMJ caused by a null mutation in the *atl* gene (Lee et al., 2009). Our results confirm these findings, but also establish a critical role for the presynaptic component of motor neurons, both at morphological and functional levels. These observations expand on previous studies that addressed the relevance of neuronal Atlastin in locomotor behavior (Summerville et al., 2016). Additionally, our findings demonstrate that expression in broad neuron circuitries, not just in motor neurons, is required to rescue the *atl*-null phenotype, providing evidence of a global susceptibility for Atlastin misfunction in the fly nervous system. Whether independent and additive effects of Atlastin in muscle and neurons explain the partial

Journal of Cell Science (2017) 130, 3507-3516 doi:10.1242/jcs.201657

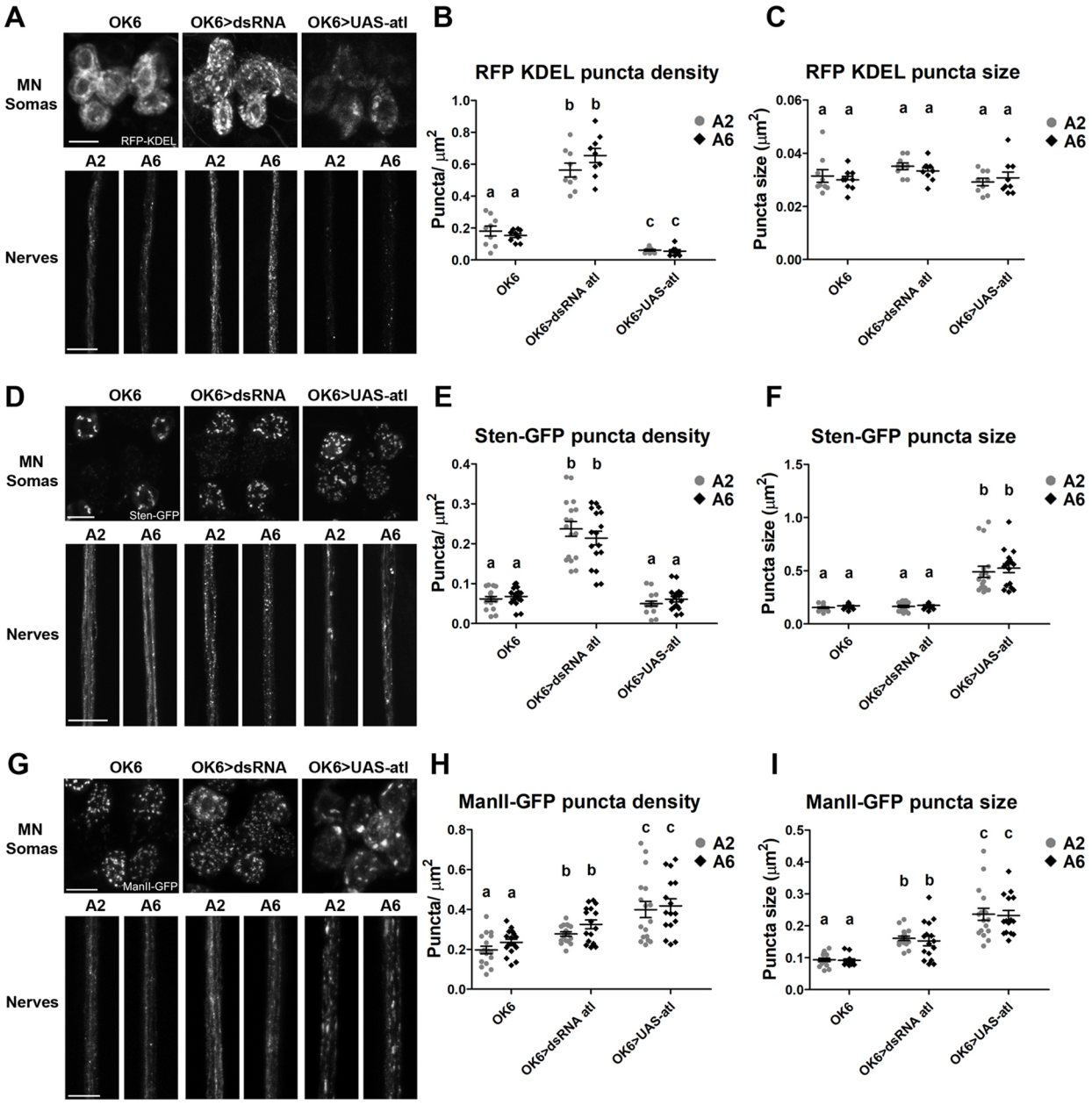

Fig. 4. Accumulation of abnormal secretory organelles in axons upon downregulation or overexpression of Atlastin. (A) *Z*-projection confocal microscopy images of motor neuron somas (upper panels) and segmental nerves (lower panels) at anterior (A2) or posterior (A6) segments in larvae expressing the ER marker RFP-KDEL and dsRNA *atl* or full-length Atlastin (UAS-Atl). (B,C) Density (B) and size (C) of RFP-KDEL puncta in A2 (gray circles) or A6 (black diamonds) segmental nerves (n=10, one-way ANOVA with post-hoc Tukey). (D) *Z*-projection of motor neuron somas (upper panels) and segmental nerves (lower panels) at anterior (A2) or posterior (A6) segments in larvae expressing the ERES marker Sten-GFP and dsRNA *atl* or full-length Atlastin (UAS-Atl). (E,F) Density (E) and size (F) of Sten-GFP puncta in A2 (gray circles) or A6 (black diamonds) segmental nerves (n=8, one-way ANOVA with post-hoc Tukey). (G) *Z*-projection of motor neuron somas (upper panels) and segmental nerves (lower panels) at anterior (A2) or posterior (A6) segments in larvae expressing the Golgi marker ManII-GFP and dsRNA *atl* or full-length Atlastin (UAS-Atl). (H,I) Density (H) and size (I) of ManII-GFP puncta in A2 (gray circles) or A6 (black diamonds) segmental nerves (n=10, one-way ANOVA with post-hoc Tukey). Data are mean±s.e.m.; lower case letters indicate statistically significant differences between categories in each plot. Scale bars: 10 µm.

contribution of both tissues to the pathogenic phenotypes, or whether more complex muscle-neuron signaling mechanisms, such as the BMP pathway, are compromised, remains to be studied. Notably, a wide number of HSP genes have been correlated with BMP signaling and supernumerary boutons, including *spastin*, *spichthyin* and *spartin* (Du et al., 2010; Wang et al., 2007; Nahm et al., 2013). Additionally, knockdown of Atlastin in *Drosophila* has been correlated with overactivation of the BMP pathway and the formation of satellite boutons (Lee et al., 2009; Summerville et al., 2016), and the involvement of Atlastin in BMP signaling has been reported in zebrafish (Fassier et al., 2010). Although BMP receptor endocytic degradation or trafficking may be affected, as with other HSP-related genes (Fassier et al., 2010; Nahm et al., 2013; Wang et al., 2007), it is still unknown precisely how Atlastin might modify BMP signaling. Interestingly, *dAcsl* mutants share common features with Atlastin knockdown larvae, including traffic jams, synaptic vesicle accumulation and satellite bouton formation as a consequence of BMP signaling defects (Liu et al., 2011, 2014).

Journal of Cell Science (2017) 130, 3507-3516 doi:10.1242/jcs.201657

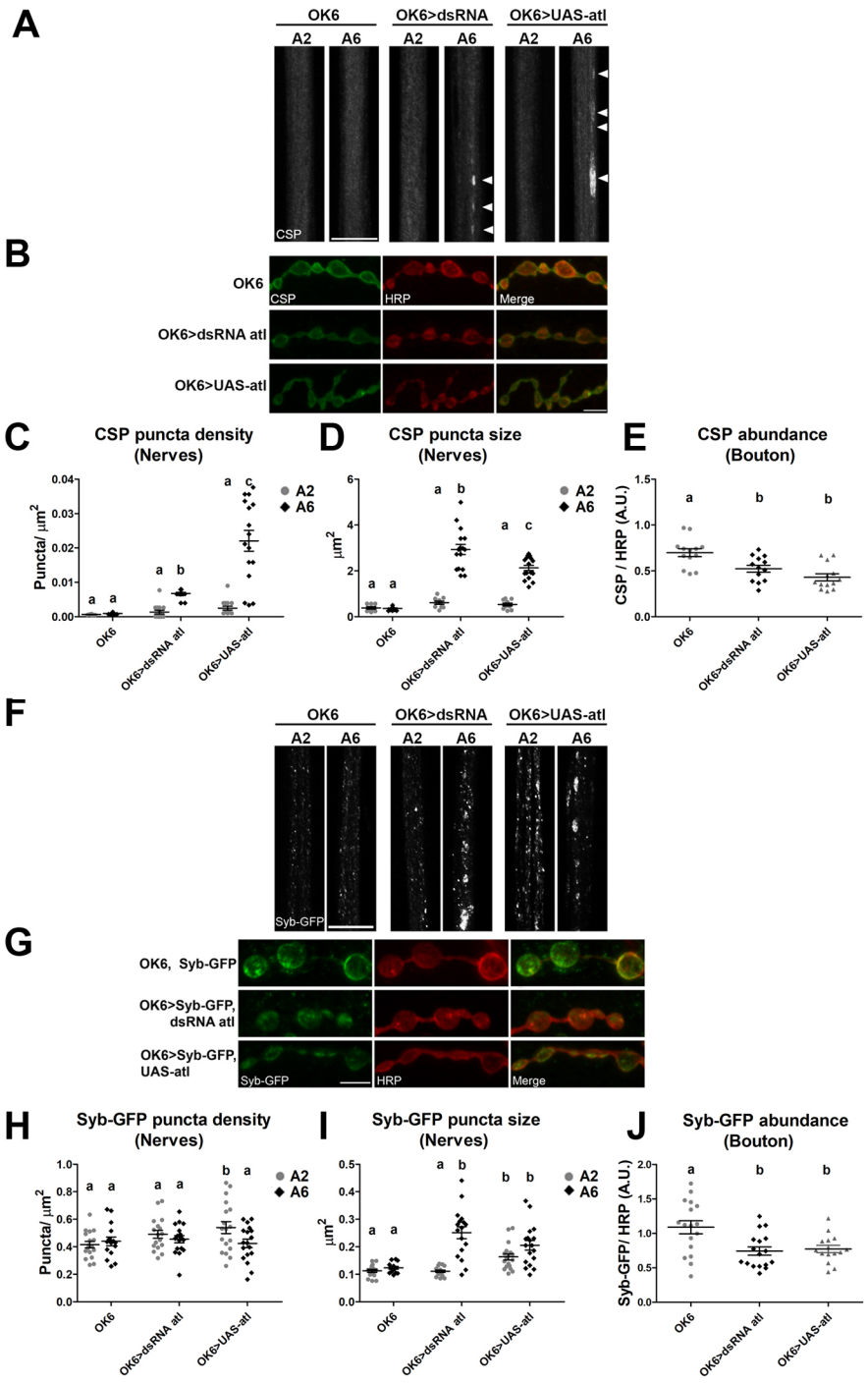

Fig. 5. Distribution of synaptic proteins in Atlastin-downregulated or -upregulated larvae. (A,B) Confocal microscopy images of segmental nerves (A) of anterior (A2) or posterior (A6) segments or synaptic boutons (B) in larvae stained with anti-CSP (green) and anti-HRP (red). Arrowheads show sites of axonal CSP accumulation. (C–E) Axonal CSP puncta density (C) and size (D), and relative abundance of CSP in boutons (E) in controls (OK6) or larvae expressing dsRNA *atl* or full-length Atlastin (UAS-Atl) (n=10, one-way ANOVA with post-hoc Tukey): (C,D) A2 (gray circles) or A6 (black diamonds); (E) OK6 (gray circles), dsRNA *atl* (black diamonds), UAS-Atl (gray triangles). (F,G) Confocal microscopy images of segmental nerves (F) at anterior (A2) or posterior (A6) segments or synaptic boutons (G) in larvae expressing the synaptic marker Syb-GFP (green) and anti-HRP (red). (H–J) Axonal Syb-GFP puncta density (H) and size (I), and relative abundance of Syb-GFP in boutons (J) in controls (OK6) or larvae expressing dsRNA *atl* or full-length Atlastin (UAS-Atl) (n=8, one-way ANOVA with post-hoc Tukey) (H–I) A2 (gray circles) or A6 (black diamonds); (J) OK6 (gray circles), dsRNA *atl* (black diamonds), UAS-Atl (gray triangles). Data are mean±s.e.m.; lower case letters indicate statistically significant differences between categories in each plot. Scale bars: 10 µm in A and F; 5 µm in B; 3 µm in G.

Light microscopy analysis showed prominent axonal aggregates of membranous organelles and synaptic components in larvae with Atlastin loss or gain of function, reminiscent of the trafficking defects described for mutations in molecular motors (Hurd and Saxton, 1996; Gindhart et al., 1998). Whether these accumulations are caused by faults in protein or lipid trafficking, protein degradation, microtubule stability or synaptic vesicle mislocalization remains to be determined. Notably, aggregates of synaptic components were more prominent in distal axons (A6 segment), where one presynaptic protein, namely CSP, co-distributed with lysosomes, revealing a length-dependent shortcoming, which is characteristic of HSPs. Poly-ubiquitinated (poly-UB) aggregates have recently been observed in *Drosophila* muscles after knockdown of neuronal Atlastin (Xu et al., 2016). Whether protein aggregates in neurons are related to these poly-UB structures remains to be determined.

Importantly, our results demonstrate that deficits in Atlastin correlate with compromises in the readily releasable and reserve pools of synaptic vesicles, and the loss of a morphologically identifiable pool of vesicles in the periphery of the AZ. Regardless of whether this occurs directly or indirectly, the relevance of these findings exceeds the pathogenesis of HSPs, and may contribute to the understanding of the cellular mechanisms of synaptic vesicle biogenesis. Intriguingly, classical reports suggest that tubo-vesicular carriers of unknown origin might contribute to the biogenesis of synaptic vesicle precursors, but the identity of these carriers has not been characterized (Droz et al., 1975; Reinecke and

Journal of Cell Science

Journal of Cell Science (2017) 130, 3507-3516 doi:10.1242/jcs.201657

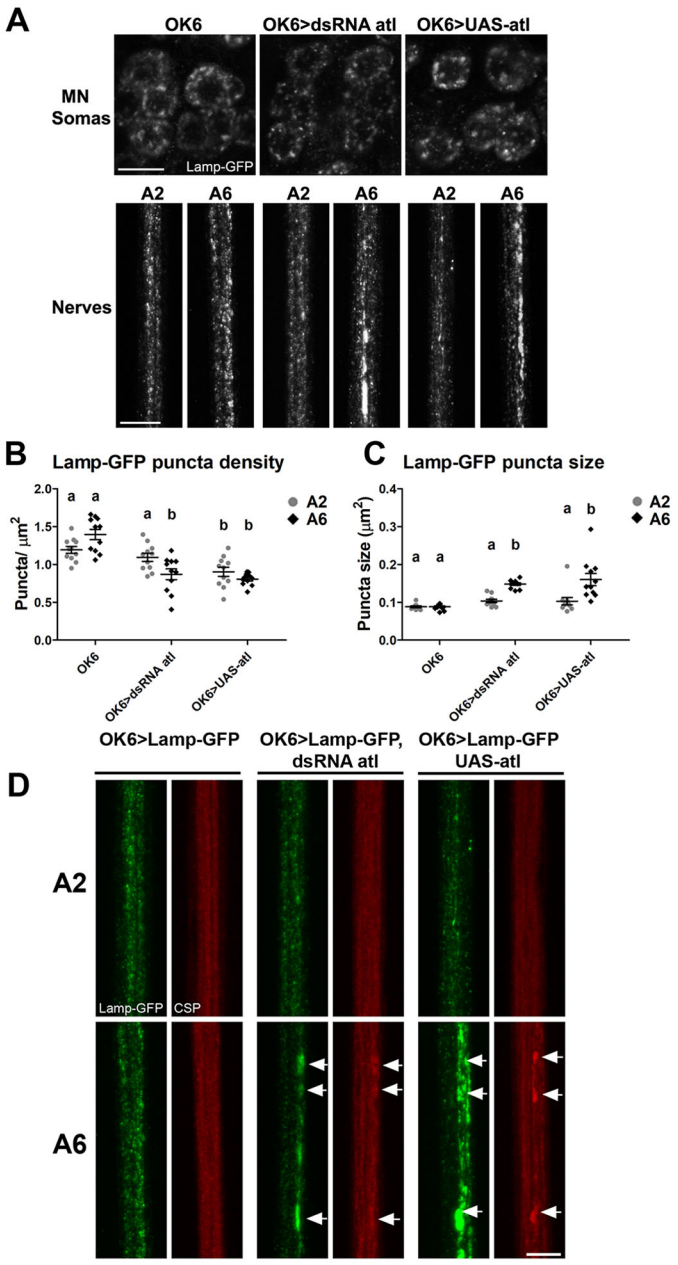

Fig. 6. Lysosomes accumulate in Atlastin-downregulated axons and co-distribute with synaptic proteins. (A) *Z*-projection confocal microscopy images of motor neuron somas (upper panels) and segmental nerves (lower panels) at anterior (A2) or posterior (A6) segments in larvae expressing the lysosomal marker Lamp-GFP and dsRNA *atl* or full-length Atlastin (UAS-Atl). (B,C) Density (B) and size (C) of Lamp-GFP puncta in A2 (gray circles) or A6 (black diamonds) segmental nerves (n=8, one-way ANOVA with post-hoc Tukey). Data are mean±s.e.m.; lower case letters indicate statistically significant differences between categories. (D) *Z*-projection of segmental nerves of anterior (A2) or posterior (A6) segments in larvae expressing the lysosomal marker Lamp-GFP and co-stained with anti-CSP. White arrows indicate co-distribution of Lamp-GFP and CSP. Images are representatives of three independent experiments (n=9 larvae). Scale bars: 10 µm in A; 5 µm in D.

Walther, 1978; Tsukita and Ishikawa, 1980; Hannah et al., 1999). Additionally, high-frequency stimulation causes synaptic vesicle depletion in motor plates, where elongated vesicles emerging from the SER may relate to the formation of synaptic vesicle precursors (Korneliussen, 1972). However, to our knowledge, no direct demonstration of this phenomenon has been reported. Under the assumption that Atlastin is present in ER and cis-Golgi compartments (Orso et al., 2009), our findings could be related to the role of the ER in synaptic vesicle formation, although the contribution of Atlastin in endocytic stages cannot be excluded. Indeed, a mutation in the *Arabidopsis* homologue RHD3 causes severe alterations in endocytic vesicles as a result of ER network defects (Stefano et al., 2015).

Synaptic developmental disorders are commonly associated with HSP mutations. The synaptic deficits described here do not fully agree with published observations (Summerville et al., 2016). Although our results are consistent with diminished neurotransmitter release during tetanic stimulation, we did not observe a reduction in evoked synaptic amplitudes under low-frequency stimulation at 1 mM [Ca^{2+}]. Voltage-clamp versus current-clamp recordings or [Mg^{2+}] differences might explain these discrepancies. Under the evoked paradigm, our findings indicate that dsRNA *atl* eliminates a single synaptic vesicle component, which is inconsistent with changes in amplitudes of evoked and miniature responses or percentage of success. Other general features, such as the overall synaptic organization, density of AZs, accumulation of large MVB-like structures, and motor deficits, are consistent in both studies and highlight the relevance of neuronal ER-shaping proteins in HSPs.

Other HSP-related proteins in *Drosophila* contribute to the understanding of the pathogenicity of the human disease. *Drosophila* has two Reticulon orthologues (*Rtnl1* and *Rtnl2*) of reticulon 1–4 in humans. Reticulons contribute to the curvature of ER membranes allowing the formation of tubules. In *Drosophila*, Rtnl1 loss of function leads to abnormalities in the distribution of the SER, the microtubule cytoskeleton and mitochondria in boutons, particularly in the distal axons or presynaptic termini of longer motor fibers (O'Sullivan et al., 2012). Likewise, *Drosophila* with loss of function of *spas* shows similar motor defects to humans with SPAST loss of function and can be rescued either by human SPAST or fly *spas* (Du et al., 2010). Moreover, expression of human mutations of SPAST in null or mutant backgrounds has allowed the generation of a powerful model with which to directly investigate the consequences of human mutations and their relevance to human disease (Du et al., 2010). Studies of *Drosophila* Spartin and Spichthyin have also provided molecular details to increase our understanding of the pathogenic mechanisms of HSPs (Sherwood et al., 2004; Trotta et al., 2004; Wang et al., 2007).

In summary, our results establish the crucial role of Atlastin in neurons, and uncover functional and morphological abnormalities in axons and presynaptic terminals that might constitute pathogenic mechanisms. They further validate *Drosophila* as an attractive organism for characterizing the cellular mechanisms underlying complex pathologies *in vivo*.

MATERIALS AND METHODS

Drosophila stocks

The following strains were used: atl^2 [kindly donated by S. Lee (Lee et al., 2009)]; UAS-dsRNA *atl* 1 (VDRC #6719 and its control W^{GD} were obtained from VDRC); UAS-dsRNA *atl* 2 (BDSC #36736); *Df(3R) Exel7357*, a deficiency that includes *atl* (BDSC #7948); two UAS-*atl*-myc independent lines, OE95 and OE64 [kindly donated by A. Daga (E. Medea Scientific Institute, Conegliano, Italy) (Orso et al., 2009)]; the motor neuron Gal4 lines OK6-Gal4 and C380-Gal4 (Sanyal, 2009) and the muscle GAL4 lines C57-GAL4 and BG487-Gal4 [kindly donated by V. Budnik (Department of Neurobiology, University of Massachusetts Medical School, Worcester, MA) (Gorczyca et al., 2007)]. The following lines were obtained from BDSC: Gal4 pan-neuronal line $Elav^{C155}$-Gal4, the glutamatergic neuronal Gal4 line OK371-Gal4, the cholinergic neuronal

Gal4 line Cha-Gal4, balancers w;If/CyO, w;If/CyO-GFP and w;MKRS/TM6b, GFP-KDEL and RFP-KDEL (ER markers), ManII-GFP (mid-Golgi marker), Rab5-GFP (early endosome marker), mito::GFP (mitochondria marker), LAMP-GFP (lysosomes marker) and the control WT line W^{1118}. Sten-GFP line ER exit site (ERES) marker was kindly donated by S. Lusching (Institute of Zoology, Universität Zürich, CH-8057 Zürich, Switzerland) (Förster et al., 2010).

Real-time qPCR

Total RNA was extracted from 10 larval brains per genotype with TRIzol reagent (Invitrogen) according to the manufacturer's protocol. Reverse transcription was performed using GoScript™ Reverse Transcriptase kit (Promega) with 500 ng total RNA for each reaction. qPCR was performed in a Stratagene MX3000P qPCR system, using the DNA binding dye SYBR Green (Agilent Technologies). Atlastin amplification was performed using the following primers: Forward, 5′-ACTTCGCCTGCGCCGTCATC-3′ and Reverse, 5′-TGGGTCGCATGAATTTCTCCCACA-3′. The ribosomal gene *Rpl32* was used as normalization control with the following primers: Forward, 5′-TGACCATCCGCCCAGCATACA-3′ and Reverse, 5′-TTGGGCTTGCGCCATTTGTG-3′. Dissociation curves were analyzed to verify the purity of products. All samples were run in triplicate.

Antibodies

Antibodies against GFP (A11122, 1:1000, Invitrogen), BRP (nc82 1:100, DHSB), CSP (6D6, 1:100 DHSB), MYC, (1:300, Sigma-Aldrich), DLG (4F3, 1:300, DHSB), HRP 647 (323-605-021) and 594 (323-585-021, both 1: 1:300, Jackson ImmunoResearch Laboratories) were purchased from the corresponding sources and used according to instructions from providers. Fluorescent secondary antibodies (FITC, CY3 and CY5) were purchased from Jackson ImmunoResearch.

Immunofluorescence and image quantification

Dissections of body wall and immunofluorescence were performed as described (Gorczyca et al., 2007). Imaging was performed on a spectral Olympus FluoView FV1000 confocal microscope (Center Valley) with a UPLSAPO 60×/1.35 NA objective and 3× digital zoom. Confocal images were acquired with sequential acquisition settings and KALMAN2 at 2048×2048 pixel resolution. Maximum *z*-series projections of five to 10 images were used. All conditions and parameters (objective, laser power, pinhole, gain, etc.) were kept constant for a particular type of experiment (e.g. KDEL in control, OK6>dsRNA, OK6>UAS-Atl). For quantification of confocal images, eight to 10 animals from three independent crosses from each genetic background were used. We used two hemisegments and at least two nerves per animal for image quantification.

For bouton number quantification, third instar larvae were labeled with anti-HRP and anti-DLG, and the total number of synaptic boutons on muscles 6/7 were counted in segment A2. Satellite boutons were defined as extensions of one or two boutons that branched off the nerve (Miller et al., 2012). Statistical significance was determined using one-way ANOVA with post-hoc Tukey. Quantification of organelle density and size, and the average intensity of fluorescent signals in axons, was determined using ImageJ (modified from Kapitein et al., 2010). HRP staining was used to normalize fluorescence intensity. Statistical significance was determined using one-way ANOVA with post-hoc Tukey.

Behavior

Larvae locomotion assays were conducted on agar plates in age-synchronized third instar larvae with feeding behavior as described (Sigrist et al., 2003). For adult climbing assays, three glass vials, each containing four age-synchronized flies per genotype were analyzed. Vials were gently tapped and flies were allowed to climb to the top of the vial (10 cm). The number of flies used for behavioral experiments was estimated using the formula $n=[t]^2\times2\times\text{variance}/(\text{difference to be detected})^2$. We used the maximum variance observed among all the genotypes, with $P=0.05$ and a certainty of 90%. We set the difference to be detected as a 20% of the mean of the control genotype. For the larval experiments, the calculated numbers were 10 for contraction frequency and 13 for larval speed. For adult climbing assays, we set to detect a 30% difference of the mean of the control genotype; thus, we calculated a number of 16 to 20, depending on the time point (van Emden, 2008). For experiments with larvae, 18–25 animals from three or four independent crosses were used; 36 animals from three independent crosses were used for adult assays. Time was recorded for each fly using a Canon EOS 550D digital camera. All assays were carried out at room temperature (RT), but larvae and adult flies were grown at 29°C to enhance the UAS-GAL4 system efficiency (Duffy, 2002), except for the Atlastin rescue experiments, in which the larvae were grown at 21°C to avoid the locomotor defects caused by Atlastin overexpression.

Electron microscopy

Longitudinal ultra-thin sections and electron micrographs were provided by the EM Core Facility, Harvard Medical School. Briefly, third instar body wall dissections were fixed for 2 h at RT with FGP fixative, containing 1.25% formaldehyde, 2.5% glutaraldehyde and 0.03% picric acid, followed by several rinses with cacodylate buffer (pH 7.4). Samples were cut into 1–2 mm cubes in the fixative, washed three times in cacodylate buffer and treated with 1% osmium tetroxide/1.5% potassium ferrocyanide (in H_2O) for 1 h at RT. Samples were washed in H_2O, then washed three times in maleate buffer (pH 5.15), before washing in 1% uranyl acetate in maleate buffer for 30 min, and washing another three times in maleate buffer. Samples were dehydrated at 4°C in 50%, 70%, 95% ethanol, warmed to RT, then in 100% ethanol twice for 15 min and propyleneoxide for 1 h. Finally, samples were infiltrated in Epon mixed 1:1 with propyleneoxide at RT for 2–3 h, moved to embedding mold filled with freshly mixed Epon, allowed to sink, and moved to oven for polymerization for 24–48 h at 60°C. Sections were cut at 60 nm, stained with 0.2% lead citrate and imaged on a JEOL 1200EX. For quantitative analyses, at least 39 images from eight larvae were analyzed per condition.

Electrophysiology

All experiments were carried out under voltage-clamp conditions on muscle 6/7 using a two-electrode voltage clamp amplifier (OC-725, Warner Instruments). sEPSCs were recorded or eEJPs induced by nerve electrical stimulation were elicited through a programmable stimulator (Master 8, AMPI), controlled by pClamp 9 software (Molecular Devices) to modify the stimulus frequency as well as the acquisition current records by means of an A/D converter. 10 MΩ resistance borosilicate electrodes filled with 3 M KCl were used to voltage hold the postsynaptic cell at −80 mV. The properties of *Drosophila* neuromuscular junction were tested in HL3.1 solution (Feng et al., 2004), consisting of 70 mM NaCl, 5 mM KCl, 4 mM $MgCl_2$, 10 mM $NaHCO_3$ 5 mM trehalose, 115 mM sucrose and 5 mM HEPES (pH 7.1), containing 1 mM $CaCl_2$; or Jan&Jan solution (Jan and Jan, 1976), consisting of 128 mM NaCl, 2 mM KCl, 4 mM $MgCl_2$, 35.5 mM sucrose and 5 mM HEPES (pH 7.1), containing 1 mM $CaCl_2$. Data analysis was performed using pClamp10 (Molecular Device). Sigmaplot10 (Systat Software) and Prisma 6 (GraphPad) were used for statistics.

Acknowledgements

We thank Drs Andrea Daga, Seunbok Lee, Vivian Budnik and Stefan Lusching for providing fly lines. We are grateful to Vivian Budnik for scientific and technical advice, and for access to facilities at University of Massachusetts Medical School.

Competing interests

The authors declare no competing or financial interests.

Author contributions

Conceptualization: C.D.G., J.S., A.C.; Methodology: C.D.G., J.S., A.C.; Validation: C.D.G., R.D., A.I.; Formal analysis: C.D.G., R.D.; Investigation: C.D.G., R.D., A.I.; Resources: J.S., A.C.; Writing - original draft: A.C.; Writing - review & editing: C.D.G., J.S., A.C.; Supervision: J.S., A.C.; Funding acquisition: J.S., A.C.

Funding

This work was supported by Comisión Nacional de Investigación Científica y Tecnológica (USA2013-020 to J.S. and A.C.) and Iniciativa Científica Milenio (P09-015-F to J.S. and A.C.).

Supplementary information

Supplementary information available online at
http://jcs.biologists.org/lookup/doi/10.1242/jcs.201657.supplemental

References

Beetz, C., Johnson, A., Schuh, A. L., Thakur, S., Varga, R.-E., Fothergill, T., Hertel, N., Bomba-Warczak, E., Thiele, H., Nürnberg, G. et al. (2013). Inhibition of TFG function causes hereditary axon degeneration by impairing endoplasmic reticulum structure. *Proc. Natl. Acad. Sci. USA* **110**, 5091-5096.

Blackstone, C. (2012). Cellular pathways of hereditary spastic paraplegias. *Annu. Rev. Neurosci.* **35**, 25-47.

Borgese, N., Francolini, M. and Snapp, E. (2006). Endoplasmic reticulum architecture: structures in flux. *Curr. Opin. Cell Biol.* **18**, 358-364.

Delgado, R., Maureira, C., Oliva, C., Kidokoro, Y. and Labarca, P. (2000). Size of vesicle pools, rates of mobilization, and recycling at neuromuscular synapses of a Drosophila mutant, shibire. *Neuron* **28**, 941-953.

Droz, B., Rambourg, A. and Koenig, H. L. (1975). The smooth endoplasmic reticulum: structure and role in the renewal of axonal membrane and synaptic vesicles by fast axonal transport. *Brain Res.* **93**, 1-13.

Du, F., Ozdowski, E. F., Kotowski, I. K., Marchuk, D. A. and Sherwood, N. T. (2010). Functional conservation of human Spastin in a *Drosophila* model of autosomal dominant-hereditary spastic paraplegia. *Hum. Mol. Genet.* **19**, 1883-1896.

Duffy, J. B. (2002). GAL4 system in *Drosophila*: a fly geneticist's Swiss army knife. *Genesis* **34**, 1-15.

Fassier, C., Hutt, J. A., Scholpp, S., Lumsden, A., Giros, B., Nothias, F., Schneider-Maunoury, S., Houart, C. and Hazan, J. (2010). zebrafish atlastin controls motility and spinal motor axon architecture via inhibition of the BMP pathway. *Nat. Neurosci.* **13**, 1380-1387.

Feng, Y., Ueda, A. and Wu, C.-F. (2004). A modified minimal hemolymph-like solution, HL3.1, for physiological recordings at the neuromuscular junctions of normal and mutant *Drosophila* larvae. *J. Neurogenet.* **18**, 377-402.

Förster, D., Armbruster, K. and Luschnig, S. (2010). Sec24-dependent secretion drives cell-autonomous expansion of tracheal tubes in *Drosophila*. *Curr. Biol.* **20**, 62-68.

Gindhart, J. G., Jr, Desai, C. J., Beushausen, S., Zinn, K. and Goldstein, L. S. (1998). Kinesin light chains are essential for axonal transport in *Drosophila*. *J. Cell Biol.* **141**, 443-454.

González, C. and Couve, A. (2014). The axonal endoplasmic reticulum and protein trafficking: cellular bootlegging south of the soma. *Semin. Cell Dev. Biol.* **27**, 23-31.

Gorczyca, D., Ashley, J., Speese, S., Gherbesi, N., Thomas, U., Gundelfinger, E., Gramates, L. S. and Budnik, V. (2007). Postsynaptic membrane addition depends on the Discs-Large-interacting t-SNARE Gtaxin. *J. Neurosci.* **27**, 1033-1044.

Guelly, C., Zhu, P.-P., Leonardis, L., Papić, L., Zidar, J., Schabhüttl, M., Strohmaier, H., Weis, J., Strom, T. M., Baets, J. et al. (2011). Targeted high-throughput sequencing identifies mutations in atlastin-1 as a cause of hereditary sensory neuropathy type I. *Am. J. Hum. Genet.* **88**, 99-105.

Hannah, M. J., Schmidt, A. A. and Huttner, W. B. (1999). Synaptic vesicle biogenesis. *Annu. Rev. Cell Dev. Biol.* **15**, 733-798.

Hu, J., Shibata, Y., Voss, C., Shemesh, T., Li, Z., Coughlin, M., Kozlov, M. M., Rapoport, T. A. and Prinz, W. A. (2008). Membrane proteins of the endoplasmic reticulum induce high-curvature tubules. *Science* **319**, 1247-1250.

Hu, J., Shibata, Y., Zhu, P.-P., Voss, C., Rismanchi, N., Prinz, W. A., Rapoport, T. A. and Blackstone, C. (2009). A class of dynamin-like GTPases involved in the generation of the tubular ER network. *Cell.* **138**, 549-561.

Hurd, D. D. and Saxton, W. M. (1996). Kinesin mutations cause motor neuron disease phenotypes by disrupting fast axonal transport in *Drosophila*. *Genetics* **144**, 1075-1085.

Jan, L. Y. and Jan, Y. N. (1976). Properties of the larval neuromuscular junction in Drosophila melanogaster. *J. Physiol.* **1**, 189-214.

Kapitein, L. C., Schlager, M. A., Kuijpers, M., Wulf, P. S., van Spronsen, M., MacKintosh, F. C. and Hoogenraad, C. C. (2010). Mixed microtubules steer dynein-driven cargo transport into dendrites. *Curr. Biol.* **20**, 290-299.

Klebe, S., Stevanin, G. and Depienne, C. (2015). Clinical and genetic heterogeneity in hereditary spastic paraplegias: from SPG1 to SPG72 and still counting. *Rev. Neurol.* **171**, 505-530.

Korneliussen, H. (1972). Ultrastructure of normal and stimulated motor endplates with comments on the origin and fate of synaptic vesicles. *Z. Zellforsch. Mikrosk. Anat.* **130**, 28-57.

Lee, Y., Paik, D., Bang, S., Kang, J., Chun, B., Lee, S., Bae, E., Chung, J. and Kim, J. (2008). Loss of spastic paraplegia gene Atlastin induces age-dependent death of dopaminergic neurons in *Drosophila*. *Neurobiol. Aging* **29**, 84-94.

Lee, M., Paik, S. K., Lee, M. J., Kim, Y. J., Kim, S., Nahm, M., Oh, S. J., Kim, H. M., Yim, J., Lee, C. J. et al. (2009). *Drosophila* Atlastin regulates the stability of muscle microtubules and is required for synapse development. *Dev. Biol.* **330**, 250-262.

Liu, Z., Huang, Y., Zhang, Y., Chen, D. and Zhang, Y. Q. (2011). *Drosophila* Acyl-CoA synthetase long-chain family member 4 regulates axonal transport of synaptic vesicles and is required for synaptic development and transmission. *J. Neurosci.* **31**, 2052-2063.

Liu, Z., Huang, Y., Hu, W., Huang, S., Wang, Q., Han, J. and Zhang, Y. Q. (2014). dAcsl, the *Drosophila* ortholog of acyl-CoA synthetase long-chain family member 3 and 4, inhibits synapse growth by attenuating bone morphogenetic protein signaling via endocytic recycling. *J. Neurosci.* **34**, 2785-2796.

Long, A. A., Mahapatra, C. T., Woodruff, E. A., III, Rohrbough, J., Leung, H.-T., Shino, S., An, L., Doerge, R. W., Metzstein, M. M., Pak, W. L. et al. (2010). The nonsense-mediated decay pathway maintains synapse architecture and synaptic vesicle cycle efficacy. *J. Cell Sci.* **123**, 3303-3315.

McCorquodale, D. S., III, Ozomaro, U., Huang, J., Montenegro, G., Kushman, A., Citrigno, L., Price, J., Speziani, F., Pericak-Vance, M. A. and Züchner, S. (2011). Mutation screening of spastin, atlastin, and REEP1 in hereditary spastic paraplegia. *Clin. Genet.* **79**, 523-530.

Miller, D. L., Ballard, S. L. and Ganetzky, B. (2012). Analysis of synaptic growth and function in *Drosophila* with an extended larval stage. *J. Neurosci.* **32**, 13776-13786.

Montenegro, G., Rebelo, A. P., Connell, J., Allison, R., Babalini, C., D'Aloia, M., Montieri, P., Schüle, R., Ishiura, H., Price, J. et al. (2012). Mutations in the ER-shaping protein reticulon 2 cause the axon-degenerative disorder hereditary spastic paraplegia type 12. *J. Clin. Invest.* **122**, 538-544.

Nahm, M., Lee, M.-J., Parkinson, W., Lee, M., Kim, H., Kim, Y.-J., Kim, S., Cho, Y. S., Min, B.-M., Bae, Y. C. et al. (2013). Spartin regulates synaptic growth and neuronal survival by inhibiting BMP-mediated microtubule stabilization. *Neuron* **77**, 680-695.

Novarino, G., Fenstermaker, A. G., Zaki, M. S., Hofree, M., Silhavy, J. L., Heiberg, A. D., Abdellateef, M., Rosti, B., Scott, E., Mansour, L. et al. (2014). Exome sequencing links corticospinal motor neuron disease to common neurodegenerative disorders. *Science* **343**, 506-511.

Orso, G., Pendin, D., Liu, S., Tosetto, J., Moss, T. J., Faust, J. E., Micaroni, M., Egorova, A., Martinuzzi, A., McNew, J. A. et al. (2009). Homotypic fusion of ER membranes requires the dynamin-like GTPase Atlastin. *Nature* **460**, 978-983.

O'Sullivan, N. C., Jahn, T. R., Reid, E. and O'Kane, C. J. (2012). Reticulon-like-1, the *Drosophila* orthologue of the Hereditary Spastic Paraplegia gene reticulon 2, is required for organization of endoplasmic reticulum and of distal motor axons. *Hum. Mol. Genet.* **21**, 3356-3365.

Park, S. H., Zhu, P.-P., Parker, R. L. and Blackstone, C. (2010). Hereditary spastic paraplegia proteins REEP1, spastin, and Atlastin-1 coordinate microtubule interactions with the tubular ER network. *J. Clin. Invest.* **120**, 1097-1110.

Reinecke, M. and Walther, C. (1978). Aspects of turnover and biogenesis of synaptic vesicles at locust neuromuscular junctions as revealed by zinc iodide-osmium tetroxide (ZIO) reacting with intravesicular SH-groups. *J. Cell Biol.* **78**, 839-855.

Sanyal, S. (2009). Genomic mapping and expression patterns of C380, OK6 and D42 enhancer trap lines in the larval nervous system of *Drosophila*. *Gene Expr. Patterns* **9**, 371-380.

Sherwood, N. T., Sun, Q., Xue, M., Zhang, B. and Zinn, K. (2004). *Drosophila* spastin regulates synaptic microtubule networks and is required for normal motor function. *PLoS Biol.* **2**, e429.

Shibata, Y., Voeltz, G. K. and Rapoport, T. A. (2006). Rough sheets and smooth tubules. *Cell* **126**, 435-439.

Sigrist, S. J., Reiff, D. F., Thiel, P. R., Steinert, J. R. and Schuster, C. M. (2003). Experience-dependent strengthening of *Drosophila* neuromuscular junctions. *J. Neurosci.* **23**, 6546-6556.

Stefano, G., Renna, L., Lai, Y. S., Slabaugh, E., Mannino, N., Buono, R. A., Otegui, M. S. and Brandizzi, F. (2015). ER network homeostasis is critical for plant endosome streaming and endocytosis. *Cell Discov.* **1**, 15033.

Summerville, J. B., Faust, J. F., Fan, E., Pendin, D., Daga, A., Formella, J., Stern, M. and McNew, J. A. (2016). The Effects of ER Morphology on Synaptic Structure and Function in *Drosophila melanogaster*. *J. Cell Sci.* **129**, 1635-1648.

Trotta, N., Orso, G., Rossetto, M. G., Daga, A. and Broadie, K. (2004). The hereditary spastic paraplegia gene, spastin, regulates microtubule stability to modulate synaptic structure and function. *Curr. Biol.* **14**, 1135-1147.

Tsukita, S. and Ishikawa, H. (1980). The movement of membranous organelles in axons. Electron microscopic identification of anterogradely and retrogradely transported organelles. *J. Cell Biol.* **84**, 513-530.

van Emden, H. F. (2008). *Statistics for Terrified Biologists*. Blackwell Publishing, Oxford, UK. ISBN 978-1-4051-4956-3.

Vedrenne, C. and Hauri, H.-P. (2006). Morphogenesis of the endoplasmic reticulum: beyond active membrane expansion. *Traffic* **7**, 639-646.

Voeltz, G. K., Prinz, W. A., Shibata, Y., Rist, J. M. and Rapoport, T. A. (2006). A class of membrane proteins shaping the tubular endoplasmic reticulum. *Cell* **124**, 573-586.

Wang, X., Shaw, W. R., Tsang, H. T. H., Reid, E. and O'Kane, C. J. (2007). *Drosophila* spichthyin inhibits BMP signaling and regulates synaptic growth and axonal microtubules. *Nat. Neurosci.* **10**, 177-185.

Waterman-Storer, C. M. and Salmon, E. D. (1998). Endoplasmic reticulum membrane tubules are distributed by microtubules in living cells using three distinct mechanisms. *Curr. Biol.* **8**, 798-807.

Xu, S., Stern, M. and McNew, J. A. (2016). Beneficial effects of rapamycin in a Drosophila model for hereditary spastic paraplegia. *J. Cell Sci.* **130**, 453-465.

Zhao, X., Alvarado, D., Rainier, S., Lemons, R., Hedera, P., Weber, C. H., Tukel, T., Apak, M., Heiman-Patterson, T., Ming, L. et al. (2001). Mutations in a newly identified GTPase gene cause autosomal dominant hereditary spastic paraplegia. *Nat. Genet.* **29**, 326-331.